Vol. 45, No. 3 (2023) 396-407, DOI: 10.24874/ti.1433.01.23.05

Tribology in Industry

www.tribology.rs

RESEARCH

Investigation on the Effect of Contact Area and Stress Concentration on Slurry Erosion Wear of AA6063 using Hertz contact theory and Numerical Technique

Bhushan D. Nandre[a,b] and Girish R. Desale[a,*]

[a]*CSIR-National Chemical Laboratory, Dr. Homi Bhabha Road, Pune, Maharashtra, India-411 008,*
[b]*M.E.S.College of Engineering, Pune, Savitribai Phule Pune university, Maharashtra, India- 411 001.*

Keywords:

Slurry erosion wear
Area of contact
Stress concentration
Hertz contact theory
ANSYS
Mass loss

* Corresponding author:

Girish R. Desale
E-mail: gr.desale@ncl.res.in

Received: 10 January 2023
Revised: 15 February 2023
Accepted: 8 May 2023

A B S T R A C T

The properties of the erodent, namely, size, shape, hardness, density, etc. have dominant effect on mass removal from the target material surface in slurry erosion. The area of contact of the erodent particle mainly depends on its size and shape. This further leads to variation in the stress development at the target surface due to particle impact. Therefore, it is necessary to investigate the effect of area of contact and stress concentration on the target surface due to different particles shapes and sizes. In view of this, in the present investigation AA6063 is selected as target material with three natural erodents, namely, quartz, SiC and alumina. The area of contact of impacting particle with target material surface is calculated by using Hertz contact stress theory and further determined by using ANSYS for similar conditions. The minimum area of contact of 256 µm size alumina particles with AA6063 target material has been observed around 0.82 x 10^{-4} mm^2 and 0.98 x 10^{-4} mm^2 using Hertz contact stress theory and ANSYS, respectively; which produces maximum stress concentration around 99 x 10^{-3}, MPa using both the techniques. The stress concentration results by ANSYS software are compared with Hertz stress results and the maximum percentage error in stress concentration is observed around 4.19 %. The average mass loss per particle from target material surface is observed around 1.35, 1.94 and 2.11 (x 10^{-12} g) due to impact of quartz, SiC and alumina particles, respectively. The results obtained by Hertz theory and ANSYS software are observed in line with the mass loss per particle determined experimentally. SEM micrographs reveal the material removal mechanism from target material surface.

1. INTRODUCTION

In slurry erosion wear, the kinetic energy of impacting solid particles is responsible to remove material from target surface. The slurry erosion wear mainly depends on various parameters like particle size, shape, density, hardness, velocity, etc. The effect of these parameters was studied by many investigators on erosion wear individually and also collectively [1-10]. However, it has been

reported that the material removal rate mainly depends on the stresses generated by erodent particle on target surface [11]. Thus, it is important to understand the phenomenon of stress concentration on the target surface due to impact of solid particle. The stress concentration on target material surface is determined by force exerted by impacting particle and its area of contact with target surface. The force exerted by the particle is easily determined from the velocity of the impacting particle. However, the area of contact of solid particle with target material surface is much more complex due to particle size, shape and orientation of impact. Thus, the solid particle contact radius is determined by Hertz analysis and explained in detail further.

In mechanical engineering and tribology, Hertzian contact stress is a description of the stress within mating parts. Hertz's classical theory of contact is focused primarily on non-adhesive contact where no tension force is allowed to occur within the contact area. The Hertz contact theory was used by Yan and Fischer [12] to study the rail-wheel contact problems. The real area of contact and load relationship between two objects is also critically examined by investigators and proposed some mathematical models [13-14]. Hertzian contact theory explains that the stress concentration is a function of the normal contact force, the radii of curvature and the modulus of elasticity of both bodies as shown in Fig. 1 [14].

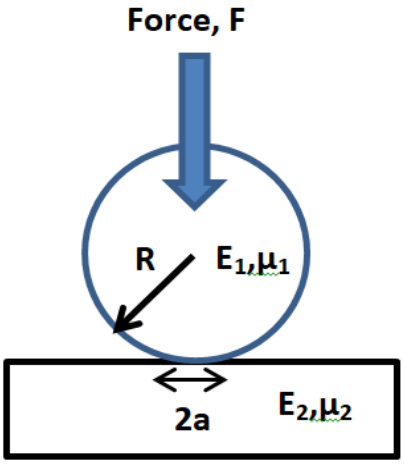

Fig. 1. Contact between a sphere and a flat plate [14].

Calculation for Equivalent modulus of elasticity E* [14],

$$\left(\frac{1}{E^*}\right) = \frac{1-v_1^2}{E_1} + \frac{1-v_2^2}{E_2} \quad (1)$$

Where, E_1 and E_2 are Young's Modulus $\boldsymbol{v}_1$ and $\boldsymbol{v}_2$ are Poisson's Ratio for two contacting bodies. Equivalent radius of two surfaces R_e, [14]

$$\left(\frac{1}{R_e}\right) = \left(\frac{1}{R_1}\right) + \left(\frac{1}{R_2}\right) \quad (2)$$

Where, R_1 and R_2 are radii of two objects, if one object is flat surface (i.e. infinity radius of curvature), Hence, $R_e = R$ (Radius of spherical object).

The force acting on target surface is calculated using relationship [15],

$$\begin{aligned} Force &= mass \times acceleration \\ &= \text{volume} \times \text{density} \times \text{acceleration} \\ &= \left(\frac{4}{3}\right)\pi r^3 * \rho * \frac{V^2}{(2*S)} \end{aligned} \quad (3)$$

Where, r, ρ, v are radius, density and velocity of erodent, respectively and S is displacement of particle.

Radius of Hertz contact area is calculated by using equation used by Xiaoyin Zhu [14],

$$a = \left[\frac{3 \times Re \times F}{2E^*}\right]^{1/3} \quad (4)$$

Where, F is Force acting on contact surface, Re is Equivalent contact radius of two surfaces, E* is Equivalent modulus of elasticity.

Accordingly, intensity of Hertz stress is calculated by using following equation [14];

$$\text{Stress: } (\sigma c)\, max = 0.4\left(\frac{E^2 F}{R^2}\right)^{1/3} \quad (5)$$

Many investigators have given more emphasis to the individual parameters namely, target material properties, solid particle properties, its size, shape, velocity, impacting angle, etc. for prediction of erosion wear [1-10]. Moreover, efforts have been made by many other investigators to determine the kinetic energy (volume, density, velocity) of impacting particles to correlate with erosion wear (mass loss) [15-17]. However, the kinetic energy of impacting particle does not include the effect of particle shape, area of contact, poison's ratio, young's modulus, etc. Thus, the Hertz contact theory approach looks more appropriate to investigate the erosion wear.

Additionally, various modern techniques like ANSYS and CFD FLUENT have been used by researchers to investigate erosive wear in engineering geometries which are characterized by a finite number of parameters [18-24]. Wang et al. [18] have developed a sole numerical model to simulate the stick-slip contact of two elastically similar surfaces. Bharat Bhushan [19] has examined the contact modeling of two rough surfaces under normal approach to predict the real area of contact which affects friction and wear of an interface. CFD numerical method was used to analyse the flow field in pumps to determine pressure, velocity, kinetic energy, shear stress, etc. under different operation conditions [20-22]. Many Investigators have also studied the Hertz contact stress analysis and validation of results using Finite Element Analysis [23-24].

Accordingly, in the present investigation three natural erodents, namely, Quartz, SiC and Alumina having four different sizes are used to impact on AA6063 target material. The kinetic energy of all the impacting particles is kept constant around 5.74×10^{-7} J by varying velocity of particles with respective to density and size. The areas of contacts of these erodents with AA 6063 specimen surface are determined by using Hertz contact theory and numeric technique. Further, the stresses generated on AA6063 material due to impact of all three erodent are determined and compared with mass loss per particle.

2. PROPERTIES OF MATERIALS

In the present investigation, AA6063 is used as target material for erosion wear and its elemental composition is given in Table 1. The hardness of AA6063 is observed around 91 HV. The value of Modulus of elasticity is 88.5 GPa and Poisson's ratio 0.334 is taken from manufactures catalogue.

Table 1. Elemental composition of AA 6063.

Element	Cu	Fe	Zn	Mn	Si	Cr	Mg	Ti	Al
Content (%)	0.013	0.24	0.01	0.055	0.389	0.015	0.510	0.008	Bal. (98.76)

The three natural solid particles namely, Quartz, SiC and Alumina are used as erodents with four different sizes 256 μm, 362.5 μm, 462.5 μm and 550 μm for the present investigation. The physical properties density, hardness, Poisson's ratio and modulus of elasticity, etc. of all these three erodents are given in Table 2. It is observed that the density and Young's modulus of alumina particles is higher where hardness and Poisson's ratio of SiC particle is maximum among all three erodents. Additionally, the shape factor values of 15 particles of each erodent have been used to calculate the average particle shape factor values of three erodents and are given in Table 2. The particle shape factor is defined between 0-1, the lower value of particle shape factor indicates more angularity in nature and approaching to 1 specify its roundness. It is observed that the shape factor of alumina particles is 0.3425 confirms its more angularity compare to SiC and quartz particles. For better understanding SEM images of all three natural erodents with particle size 256 μm are shown in Fig. 2 (a-c).

(a) Quartz (b) SiC (c) Alumina

Fig. 2. SEM images of Erodent of size 256 μm.

Table 2. Erodent's properties (manufactures catalogue).

Solid Particle	Colour	Density, Kg/m3	Hardness, Hv	Particle Shape factor	Poisson's Ratio	Modulus of Elasticity, GPa
Quartz (SiO2)	White	2652	1100	0.7007	0.17	97.2
Silicon carbide (SiC)	Blackish	3210	2500	0.4425	0.35	90
Alumina (Al2O3)	Brown	3970	1800	0.3425	0.21	215

3. AREA OF CONTACT AND STRESS CONCENTRATION BY THEORETICAL AND NUMERICAL TECHNIQUE

The critical examination of all physical properties of three natural erodents reveals that the estimation of slurry erosion wear is a complex phenomenon. However, in the present investigation the stress concentration on the target material surface due to impact of solid particle is given more emphasis and used to compare with erosion wear data. It is reported that the shape of impacting particles (angularity or shape factor) has dominant effect on mechanism of material removal from the target surface [25-26]. Increasing the angularity of the solid particles decreases the area of contact with target material surface as shown in Fig. (3).

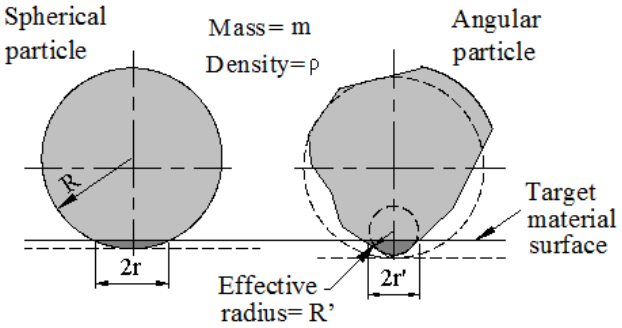

Fig. 3. Contact area of spherical and angular erodent with flat surface [25].

Thus, the particle shape factor has been considered to determine the effective radius of the solid particle and its contact area with target material surface. Further, Hertz contact theory and numeric technique (ANSYS) are used to determine the stress concentration developed at target surface.

3.1 Using Hertz contact theory

The equivalent modulus of elasticity E* is calculated by using equation 1, for all three natural erodent's namely quartz, SiC and alumina. Sample calculation is given below for quartz particle;

Poisson's ratio for quartz (v_1) = 0.17

Poisson's ratio for AA6063 (v_2) = 0.334

Modulus of elasticity for quartz (E_1) = 97.2 GPa

Modulus of elasticity for AA6063 (E_2) = 88.5 GPa

Contact Modulus,

$$\frac{1}{E^*} = \frac{1-{v_1}^2}{E_1} + \frac{1-v_2^2}{E_2}$$

$$\frac{1}{E^*} = \frac{1-0.17^2}{97.2} + \frac{1-0.334^2}{88.5}$$

$$E^* = 49.925 \text{ GPa}$$

The equivalent radius (Re) is taken as the radius of spherical object since the other contact surface (target specimen AA6063) is flat. All the three natural erodents are having different shape factors as given in Table 2. Hence, the equivalent radius Re is calculated by multiplying respective shape factor of individual erodent with the particle size. The forces acting due to impact of three erodents on the target surface are calculated by using equation 3, where mass and acceleration of individual particle are calculated from particle size, density and velocity as per Table Nos. 2 and 3.

Force of quartz particle (d= 256μm)

F = mass x acceleration

= volume * density * acceleration

$$= \left(\frac{4}{3}\right) * \pi r^3 * \rho * \frac{V^2}{(2*S)}$$

$$= \left(\frac{4}{3}\right) * \pi (0.128 * 10^{-3})^3 * 2652 * \frac{(7.02)^2}{(2*0.071)}$$

F = 8.084 x10^{-6} N

The kinetic energy of all particles kept constant by varying velocities as shown in Table 3. The areas of contacts of all three natural erodents with the target surface are calculated using equation 4 and presented in Table 3. Finally, the stresses generated on AA6063 specimen surface due to impact of three natural erodents are calculated by using equation 5 and presented in Table 3.

Table 3. Area of contact and stresses developed on AA6063 specimen surface due to impact of all three natural erodents by using Hertz Contact Theory and ANSYS software.

Type of erodent and shape factor	Particle Size, μm	Velocity of particles, m/s	Hertz Contact Theory		Numerical Technique (ANSYS)		% Stress Error
			Area of contact (x 10^{-4}), mm^2	Stress (x10^{-3}), MPa	Area of contact by ANSYS (x 10^{-4}), mm^2	Stress by ANSYS (x10^{-3}), MPa	
Quartz (0.7007)	256	7.02	1.75	46.21	1.89	47.20	2.14
	362.5	4.16	1.99	40.44	2.13	41.96	3.76
	462.5	2.89	2.16	37.33	2.21	38.26	2.49
	550	2.23	2.26	35.87	2.30	36.85	2.73
SiC (0.4425)	256	6.38	1.10	73.45	1.25	74.98	2.08
	362.5	3.78	1.23	65.28	1.26	66.35	1.64
	462.5	2.62	1.34	60.09	1.39	61.58	2.48
	550	2.02	1.42	57.03	1.52	59.42	4.19
Alumina (0.3425)	256	5.73	0.82	99.11	0.98	99.96	0.86
	362.5	3.4	0.90	90.10	1.00	90.85	0.83
	462.5	2.36	1.01	80.20	1.12	82.65	3.05
	550	1.82	1.09	73.96	1.15	75.03	1.45

The variation in the area of contact of different particles shapes and sizes with AA6063 target material surface using Hertz contact theory are graphically presented in Fig. 4. It is observed from Fig. 4 that the area of contact calculated by Hertz theory increases with increasing particle size and shape factor. The biggest Hertz area of contact of blocky shape 550 μm size quartz particles (S.F. 0.7007) with target material surface is observed about 2.26 x 10^{-4} mm^2 compare to sub angular shape SiC (S.F. 0.4425) and angular shape alumina particles (S.F. 0.3425). Finally, the stresses generated by different solid particles (erodents) on AA6063 target material surface are presented graphically in Fig. 5. It has been observed that the stress concentration on target specimen decreases with increasing particle shape factor for all size of particles. It is observed that the highest stress (99.11 x 10^{-3} MPa) is generated on AA6063 target material surface due to impact of 256 μm size angular shape of alumina particles (S.F. 0.3425) compare to sub angular shape SiC (S.F. 0.4425) and blocky shape quartz (S.F. 0.7007) particles. This reveals that the angular shape particles are responsible to generate higher stress on target surface compared to other erodents. It is also observed from Fig. 5 that the stress concentration on target specimen is increases with the decrease in particle size for all three erodent.

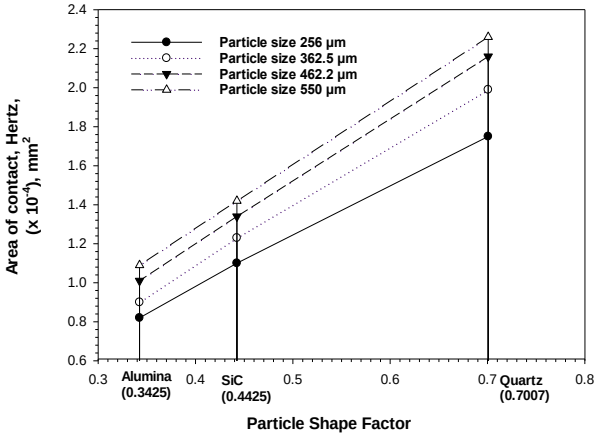

Fig. 4. Variation in the area of contact (Hertz) with different particles shape and size.

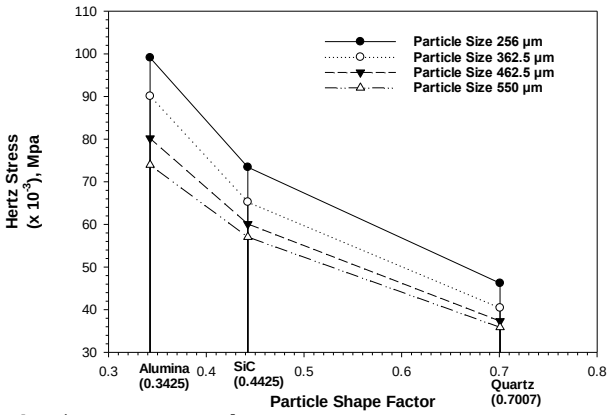

Fig. 5. Variation in the stress concentration on AA6063 material with different particles shape and size.

3.2 Using numeric technique ANSYS

The velocity conditions for all three natural erodents for different sizes are given in Table 3. These different velocity conditions are further used to simulate in ANSYS explicit dynamics software to interpret the area of contact and stress concentration on AA6063 target material surface [27].

The result interpretations for area of contact on AA6063 target material due to all four different size quartz particles are presented in Fig. 6 (a-d). It is observed from Fig. 6 (a-d) that due to impact of the particles at 90° angle initiate the crack on AA6063 material surface and further material loss is observed due to successive impacts of particles. The minimum area of contact is observed 1.89 x 10^{-4} mm^2 for 256 µm quartz particles as shown in Fig. 6(a), whereas for particle size 550 µm, area of contact is observed highest 2.30 x 10^{-4} mm^2 as shown in Fig. 6(d). It indicates that the area of contact between AA6063 plate and quartz particles increases with increase in particle size.

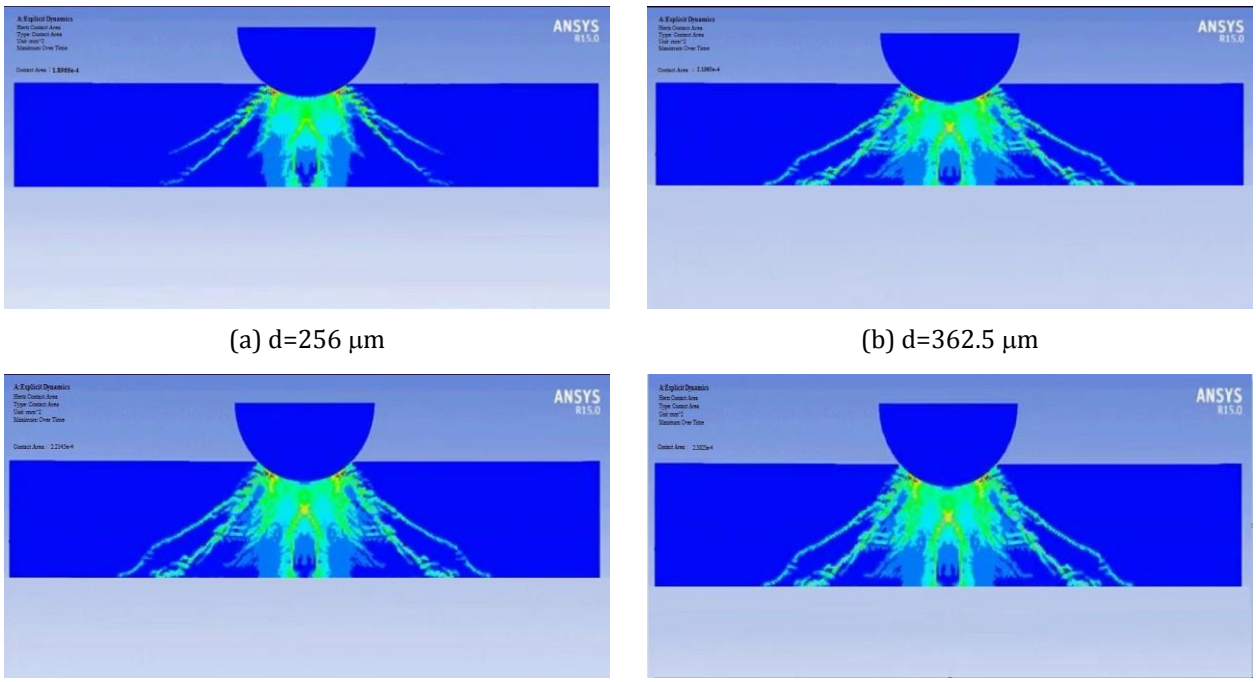

(a) d=256 µm (b) d=362.5 µm

(c) d=462.5 µm (d) d=550 µm

Fig. 6. Area of contact between AA6063 plate and four different sizes of Quartz particles using ANSYS.

However, results for stress concentrations on AA6063 target surface due to impact of all four sizes of quartz particles by using ANSYS software are shown in Fig. 7 (a-d). The maximum stress concentration due to impact of all three erodents occurs at the centre of indentation which is observed with red colour. It is observed that maximum stress developed by 256 µm quartz particle on target surface is 47.20 x 10^{-3} MPa as shown in Fig. 7 (a), whereas for particle size 550 µm minimum stress intensity is observed around 36.85 x 10^{-3} MPa as shown in Fig. 7 (d). It reveals that stress intensity is more due to impact of smaller particles due to less area of contact with the target material surface.

Furthermore, the result interpretations for area of contact and stress concentrations on AA6063 target material due to 256 µm size, SiC and alumina particles are presented in Fig. 8 (a-b), and Fig. 9 (a-b), respectively. The area of contact due to impact of three different erodents on AA6063 target material surface using ANSYS explicit dynamics software are given in Table 3 and the variation is graphically presented in Fig. 10. It is observed that the area of contact increases significantly with increasing particle shape factor for all three erodents. Similarly, the area of contact slightly increases with increasing the particle size.

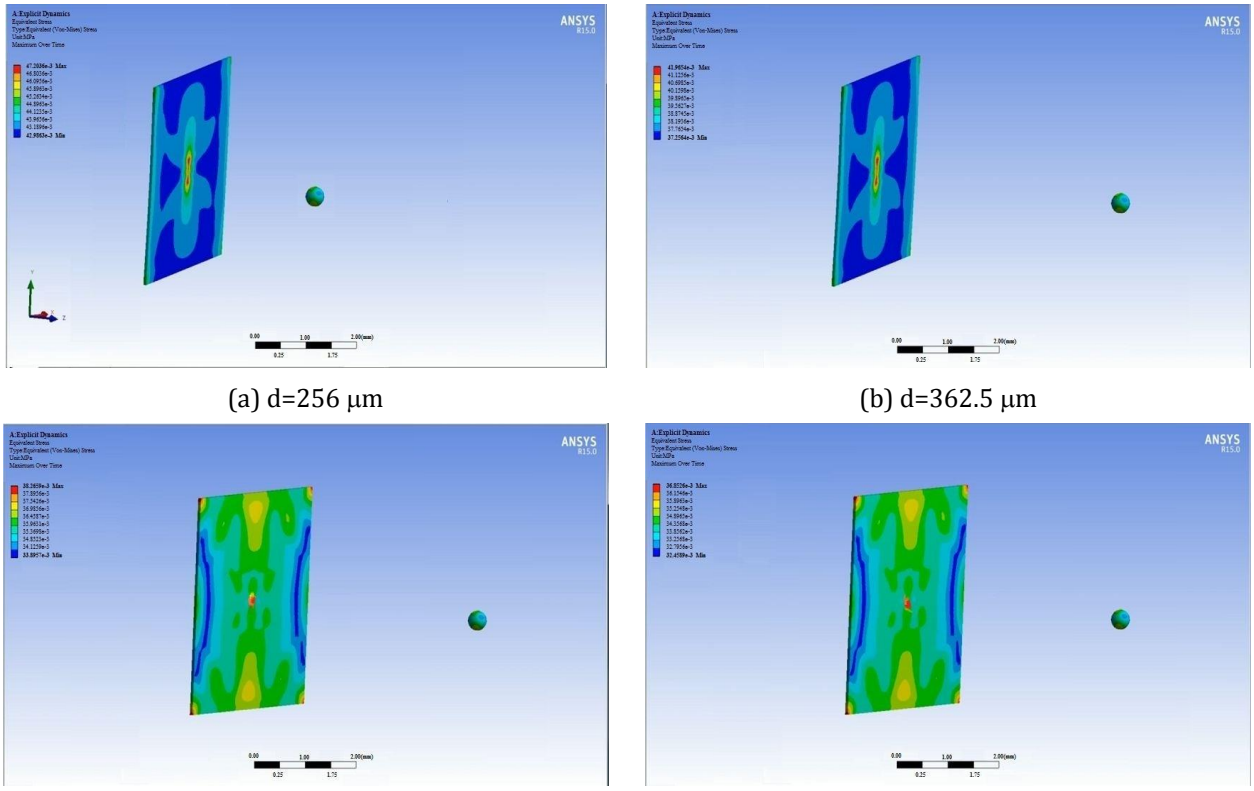

(a) d=256 μm (b) d=362.5 μm

(c) d=462.5 μm (d) d=550 μm

Fig. 7. Stresses on AA6063 plate with four different sizes of Quartz particles using ANSYS.

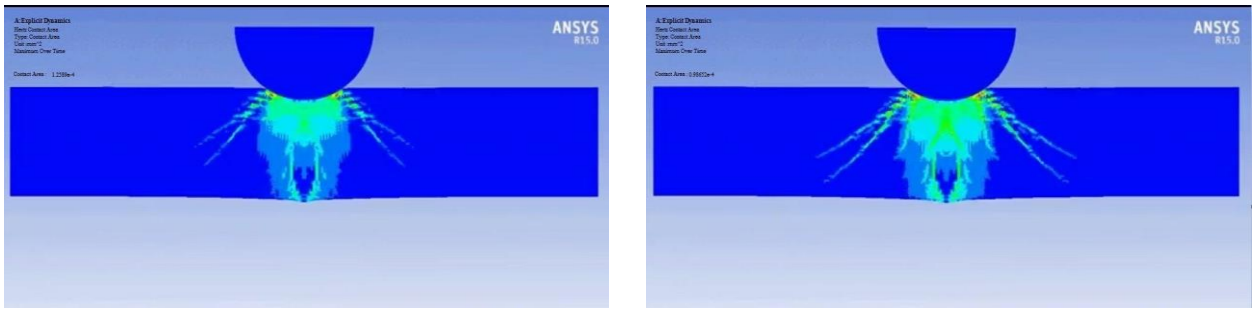

(a) SiC (b) Alumina

Fig. 8. Area of contact between AA6063 plate and erodents of size 256 μm using ANSYS software.

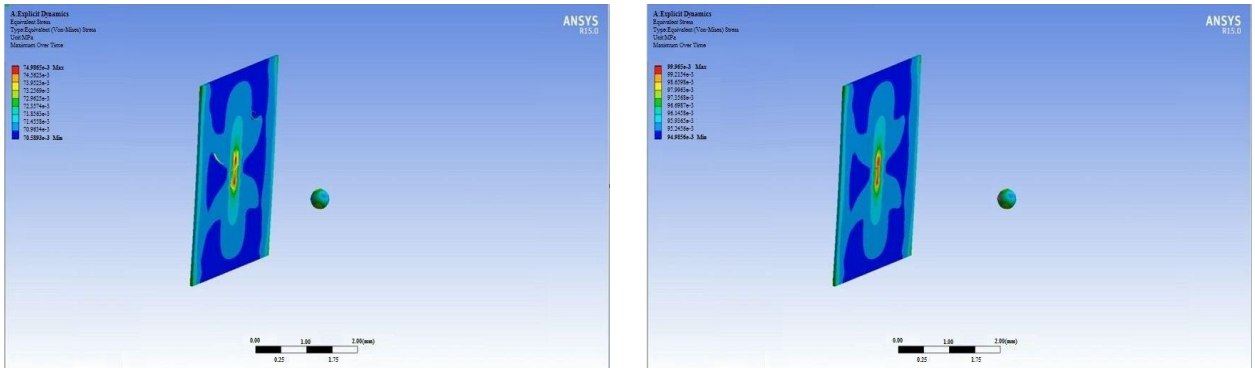

(a) SiC (b) Alumina

Fig. 9. Stresses on AA6063 plate and erodents of size 256 μm using ANSYS software.

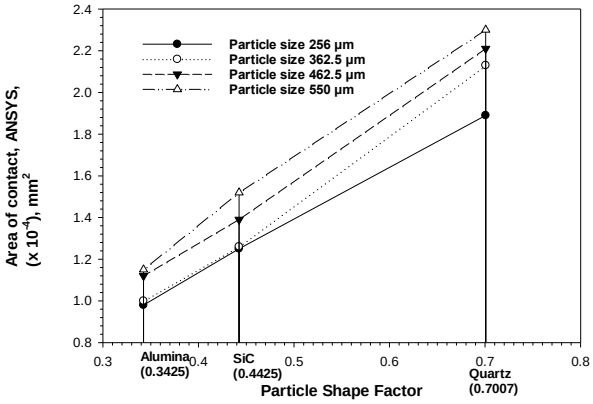

Fig. 10. Variation in the area of contact with AA6063 n

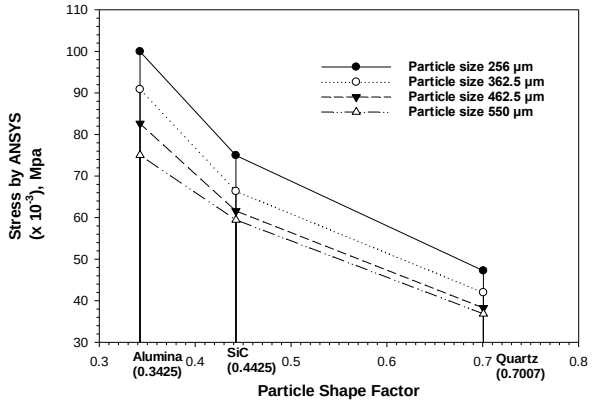

Fig. 11. Variation in stress concentration on AA6063 material using ANSYS.

The stress concentration results using ANSYS software for different erodent are graphically presented in Fig. 11. It is observed that the stress concentration decreases considerably with increasing particle shape factor. These results are well in agreement with the Hertz contact theory results of area of contact and stress concentration as shown in Fig. 4 and Fig. 5, respectively. The stress concentration results by ANSYS software are compared with Hertz stress results and given in Table 3. The maximum percentage error in stress concentration is observed around 4.19 %. P. Purushothaman et al., observed the stress error around 8.33 % between Hertz results and FEA analysis [24]. Whereas, Arulkar and Ritapure [28] observed error between experimental and artificial neural network (ANN) predicted results was around 9 %.

4. EFFECT OF AREA OF CONTACT AND STRESS CONCENTRATION ON MASS LOSS DUE TO EROSION

In order to understand the mass loss from target material surface due to slurry erosion wear, the area of contact due to impacting particle and stress concentration on target surface AA 6063 are determined analytically (Hertz contact Theory) and numerically (ANSYS) as discussed in the above sections. The experimental data on mass loss per particle from AA 6063 target material at 90° impact angle presented in the research work Nandre and Desale [15] is reused as given in Table 4 and further efforts have been made to correlate with the present objectives.

Many investigators [15-17, 29-30] have reported that the impacting particle's kinetic energy is mainly responsible to remove material from the target material surface. However, during the impact the area of contact of the particle and the stress concentration on the target material surface are different for different particle size and shape. Thus, the complete phenomena become more complex and difficult to predict.

Table 4: Range of parameters and observed mass loss per particle at 90° impact angle (23)

Erodent used	Particle Size, (µm)	Average mass of Individual particle, (kg)	Solid concentration in % by weight (Cw) in Pot	Velocity of each particle, (m/s)	Test Duration (min)	Mass Loss Per Particle, (x 10^{-12}) (g)	Avg. mass loss per particle (x 10^{-12}) (g)
Quartz	550	2.31 x 10^{-7}	30 %	2.23	42.4	1.59	1.35
	462.5	1.37 x 10^{-7}	17.83 %	2.89	32.7	1.45	
	362.5	6.61 x 10^{-8}	8.58 %	4.16	22.6	1.33	
	256	2.33 x 10^{-8}	3.02 %	7.02	13.4	1.05	
Silicon carbide (SiC)	550	2.79 x 10^{-7}	30.57 %	2.02	46.8	2.26	1.94
	462.5	1.66 x 10^{-7}	18.18 %	2.62	35.9	2.11	
	362.5	8.00 x 10^{-8}	8.75 %	3.78	24.9	1.86	
	256	2.82 x 10^{-8}	3.08 %	6.38	14.8	1.55	
Alumina (Al_2O_3)	550	3.46 x 10^{-7}	35.24 %	1.82	51.9	2.45	2.11
	462.5	2.06 x 10^{-7}	20.95 %	2.36	40.0	2.17	
	362.5	9.90 x 10^{-8}	10.08 %	3.4	27.7	1.98	
	256	3.49 x 10^{-8}	3.55 %	5.73	16.4	1.86	

The variation in mass loss per particle given in Table 4 is re-plotted with the particle shape factor of the erodents in Fig. 12 (a). It is observed from Fig. 12 (a) that the angular alumina particles remove material more effectively from the target surface compare to the sub angular shape of SiC and blocky shape of quartz particles. It is reported that both the increase in angularity and the hardness of solid particles develop favourable conditions for dissipation of higher kinetic energy per unit area of the target surface [24]. However, the mass loss due to less hardness of alumina particles is more than the higher hardness of SiC particles. It reveals that the particle shape is more dominant than the hardness.

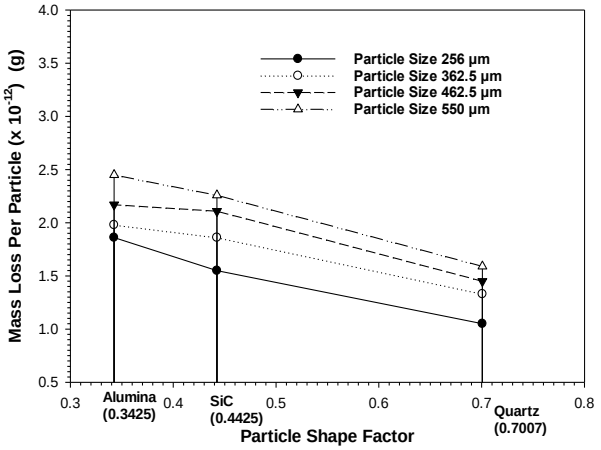

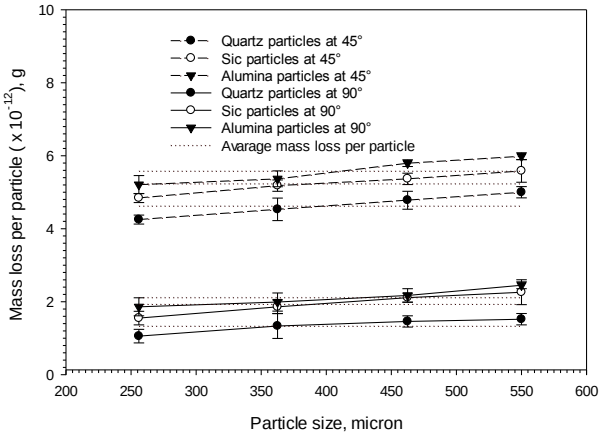

(b) Effect of Particle size [15]

Fig. 12. Variation in mass loss per particle from AA6063 specimen due to impact of different particles shape and size.

It is observed that the stress concentration on AA6063 target material surface decreases with increasing the shape factor of erodents as predicted using Hertz theory and ANSYS software as shown in Fig. 5 and 11, respectively. The alumina particles having sharp edges make small area of contact with target material surface and thus able to generate more stresses compare to other two erodents (sub angular SiC and blocky shape quartz). This higher stress concentration due to alumina particles may be responsible for maximum mass loss per particle. This is in line with the results represented in Fig. 12 (a) for mass loss per particle (15).

Similarly, the stress concentration increases slightly with decreasing the particle size for all three erodent as shown in Fig. 5 and Fig. 11. It reveals that the individual smaller size particles are responsible to generate more stress on target surface as compared to larger size particles of same kinetic energy. However, the mass loss per particle due to smaller size of particles is marginally less as compared to larger size particles for all three erodent as shown in Fig. 12 (b). This reveals that although the individual smaller size particle having tendency to generate more stress on target material surface but show less mass loss per particle compared to larger particles of same kinetic energy.

This phenomenon can be attributed to smaller size particles get entrapped in the secondary flow field and not able to hit the target material surface effectively. This is in line with the observations reported by Clark and his associates [31-33]. They have measured the number of craters and their diameters developed on the test specimen due to impact of different size particles. They have observed that the collision efficiency of impacting particles decreases sharply with decrease in particle size. Thus, though the stress generated by individual smaller size particle is higher however due to poor striking efficiency the smaller particles are unable to remove the material successfully from the target surface compare to larger size particles. This indicates that the collision efficiency of impacting particles also plays dominant role in slurry erosion wear. Recent studies also confirm the influence of flow field in cavitation and erosion wear [34-36].

5. SEM EXAMINATION

Many investigators have examined the eroded surfaces using scanning electron microscope (SEM) to understand the material removal mechanisms [37-41]. The SEM micrographs of AA6063 eroded surfaces at normal impact angle are presented in Fig 13. (a-c). It is observed from Fig. 13 (a), that the indentation craters are big in

size and rounded in shape due to blocky shape of quartz particles. While elongated craters are formed due to impact of sub angular shape SiC particles as shown in Fig. 13 (b). The material is plastically deformed to form a rim around the crater gets flattened and fractured with further successive impacts. Similar indentation craters are observed with alumina particles (Fig. 13 (c)), however the material gets removed more effectively due to sharp cutting edges.

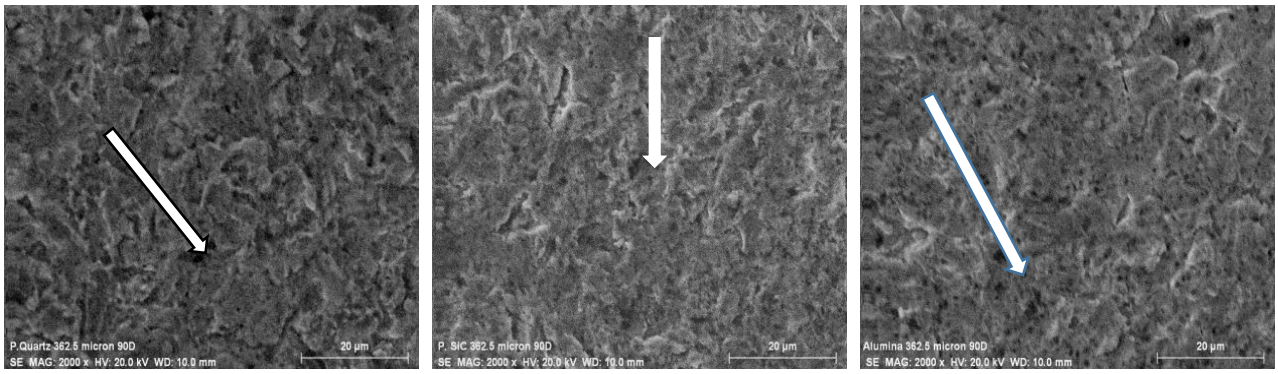

(a) Quartz (b) SiC (c) Alumina

Fig. 13: SEM images of AA6063 Target material with erodent of 362.5 µm at 90° impact angle

6. CONCLUDING REMARKS

The area of contact and stresses generated on AA6063 material surface by all three natural erodent namely, Quartz, SiC and Alumina are investigated by using Hertz contact theory and ANSYS software. These results are further compared with the mass loss per particles values. The generic conclusions drawn from present study are discussed below.

1. The area of contact of impacting particles with target material surface increases with increasing the shape factor and particle size by using both methods Hertz contact theory and ANSYS software. Thus, the maximum stress 99.11 x 10^{-3} MPa is generated on AA6063 target surface by angular shape of 256 µm size alumina particles by using Hertz contact theory and 99.96 x 10^{-3} MPa using ANSYS. Whereas, least stress 35.87 x 10^{-3} MPa is generated by blocky shape of 550 µm size quartz particles by using Hertz contact theory and 36.85 x 10^{-3} MPa using ANSYS. The stress concentration results determined by using Hertz contact theory are nearly close with ANSYS results with maximum error of 4.19 %.

2. The experimental results of mass loss per particle from AA6063 specimen are also in line with the results obtained by Hertz contact stress theory and ANSYS software with considering particle shape factor. Angular shape of alumina particles removes more material from target surface due to higher stress concentration generated by them. The average mass loss per particle due to four sizes of alumina particles is determined 2.11 x 10^{-12} g, whereas for quartz particles it is observed as 1.35 x 10^{-12} g and for SiC it is observed as 1.94 x 10^{-12} g. It reveals that the shape of striking particle plays dominant role in slurry erosion wear.

3. Although the smaller size of all three erodent having higher values of stress concentration does not able to contribute in overall mass loss from target surface due to less striking efficiency. Hence, particle size is also dominant along with particle shape in erosion wear study.

4. SEM micrograph at normal impact angle reveals the material removing mechanism from target material surface. The SEM micrograph of eroded surface due to alumina particles confirms higher material removal due to its sharp cutting edges. While the plastic deformation phenomenon becomes more dominant due to impact of blocky shape of quartz particles.

Acknowledgment

The authors gratefully acknowledge the financial support from CSIR-NCL Pune and are also thankful to Dr. Ashish Lele Director, Pune.

REFERENCES

[1] B.K. Gandhi, S.N. Singh, V. Seshadri, *Study of the parametric dependence of erosion wear for the parallel flow of solid-liquid mixtures*, Tribology International, vol. 32, iss. 5, pp. 275-282, 1999, doi: 10.1016/S0301-679X(99)00047-X

[2] M.A. Al-Bukhaiti, A. Abouel-Kasem, K.M. Emara, S.M. Ahmed, *Particle shape and size effects on slurry erosion of AISI 5117 steels*, Journal of Tribology, vol. 138, iss. 2, 2016, doi: 10.1115/1.4031987

[3] H. Adarsha, R. Keshavamurthy, S. Ramesh, Naveen P. Noronha, *Effect of Carbon Fiber Rod Reinforcement on Slurry Erosive Behavior of Al6061 Composites*, Procedia Technology, vol. 25, pp. 916-923, 2016, doi: 10.1016/j.protcy.2016.08.179

[4] S.R. More, D.V. Bhatt, J.V. Menghani, *Study of the Parametric Performance of Solid Particle Erosion Wear under the Slurry Pot Test Rig*, Tribology in Industry, vol. 39, no. 4, pp. 471-481, 2017, doi: 10.24874/ti.2017.39.04.06

[5] M. Liebhard, A. Levy, *The effect of erodent particle characteristics on the erosion of metals*, Wear, vol. 151, iss. 2, pp. 381-390, 1991, doi: 10.1016/0043-1648(91)90263-T

[6] B. Venkataraman, G. Sundararajan, *The solid particle erosion of copper at very low impact velocities*, Wear, vol. 135, iss. 1, pp. 95-108, 1989, doi: 10.1016/0043-1648(89)90098-7

[7] S. Bahadur, R. Badruddin, *Erodent particle characterization and the effect of particle size and shape on erosion*, Wear, vol. 138, iss. 1-2, pp. 189-208, 1990, doi: 10.1016/0043-1648(90)90176-B

[8] F.Y. Lin, H.S. Shao, *Effect of impact velocity on slurry erosion and a new design of a slurry erosion tester*, Wear, vol. 143, iss. 2, pp. 231-240, 1991, doi: 10.1016/0043-1648(91)90098-F

[9] S.R. More, D.V. Bhatt, J.V. Menghani, *Effect of microstructure and hardness on slurry erosion behaviour of A356 alloy using slurry pot test rig*, Transactions of the Indian Institute of Metals, vol. 72, pp. 3191-3199, 2019, doi: 10.1007/s12666-019-01784-z

[10] R. Tarodiya, B.K. Gandhi, *Experimental Investigation on Slurry Erosion Behaviour of 304L Steel, Grey Cast Iron, and High Chromium White Cast Iron*, Journal of Tribology, Vol. 141, iss. 9, 2019, doi: 10.1115/1.4043903

[11] G.R. Desale, B.K. Gandhi, S.C.Jain, *Effect of Physical Proper-ties of Solid Particle on Erosion Wear of Ductile Materials,* in World Tribology Congress III, 12-16 September, 2005, Washington, D.C., USA, pp. 149-150, doi: 10.1115/WTC2005-63997

[12] W. Yan, F. D. Fischer, *Applicability of Hertz contact theory to rail-wheel contact problems*, Article archieve of Applied Mechanicss, vol. 70, pp. 255-268, 2000.

[13] M. Ciavarella , V. Delfine, G. Demelio, *A "re-vitalized" Greenwood and Williamson model of elastic contact between fractal surfaces*, Journal of the Mechanics and Physics of Solids, vol. 54, iss. 12, pp. 2569–2591, 2006, doi: 10.1016/j.jmps.2006.05.006

[14] X. Zhu, Tutorial on hertz contact stress, available at: https://wp.optics.arizona.edu/optomech/wp-content/uploads/sites/53/2016/10/OPTI-521-Tutorial-on-Hertz-contact-stress-Xiaoyin-Zhu.pdf

[15] B.D. Nandre, G.R. Desale, *The Effects of Constant Kinetic Energy of Different Impacting Particles on Slurry Erosion Wear of AA 6063*, Journal of Tribology, vol. 140, iss. 3, pp. 1-8, 2018, doi: 10.1115/1.4038355

[16] G.R. Desale, *Study on Slurry Erosion Behavior of Ductile Type Material and Laser Cladded Surface*, Ph.D. thesis, Indian Institute of Technology Roorkee, India, 2006.

[17] P.P. Shitole, S.H. Gawande, G.R. Desale, B.D. Nandre, *Effect of Impacting Particle Kinetic Energy on Slurry Erosion Wear*, Journal of Bio Tribo Corrosion, vol. 1, 2015, doi: 10.1007/s40735-015-0028-6

[18] D. Wang, G. De Boer, A. Neville, A. Ghanbarzadeh, *A new numerical model for investigating the effect of surface roughness on the stick and slip of contacting surfaces with identical materials*, Tribology International, vol. 159, 2021, doi: 10.1016/j.triboint.2021.106947

[19] B. Bhushan, *Contact Mechanics of Rough Surfaces in Tribology: Single Asperity Contact*, Applied Mechanics Reviews, vol. 49, iss. 5, pp. 275–298, 1996, doi: 10.1115/1.3101928

[20] A.R. Al-Obaidi, *Numerical Investigation of Flow Field Behaviour and Pressure Fluctuations within an Axial Flow Pump under Transient Flow Pattern Based on CFD Analysis Method*, Journal of Physics: Conference Series, vol. 1279, First International Scientific Conference Al-Ayen University, 30–31 March, 2019, Thi-Qar, Iraq, DOI 10.1088/1742-6596/1279/1/012069

[21] A.R. Al-Obaidi, A.A. Mohammed, *Numerical Investigations of Transient Flow Characteristic in Axial Flow Pump and Pressure Fluctuation Analysis Based on the CFD Technique*, Journal of Engineering Science and Technology Review, vol. 12, iss. 6, pp. 70–79, 2019, DOI: 10.25103/jestr.126.09

[22] B. Wu , X. Wang, X. Liu, G. Xu, S. Zhu, *Numerical simulation of erosion and fatigue failure the coal gangue paste filling caused to pumping pipes*, Engineering Failure Analysis, vol. 134, 022, doi: 10.1016/j.engfailanal.2022.106081

[23] L.C. Brezeanu, *Element Method on the Contact Stresses Between Two Bodies*., in 8th International Conference Interdisciplinary in Engineering, 9 to 10 October, 2014, Tirgu- Mures, Romania, pp. 177-284.

[24] P. Purushothaman, P. Thankachan, *Hertz contact stress analysis and validation using Finite Element Analysis*, International Journal for Research in Applied Science & Engineering Technology (IJRASET), vol. 2, iss. 11, pp. 531-538, 2014.

[25] G.R. Desale, B.K. Gandhi, S.C. Jain, *Effect of erodent properties on erosion wear of ductile type materials*, Wear, vol. 261, iss. 7-8, pp. 914–921, 2016, doi: 10.1016/j.wear.2006.01.035

[26] S. Leguizamóna, E. Jahanbakhsha,b, S. Alimirzazadeha, A. Maertensa, F. Avellan, *FVPM numerical simulation of the effect of particle shape and elasticity on impact erosion*, Wear, vol. 430–431, pp. 108–119, 2019, doi: 10.1016/j.wear.2019.04.023

[27] Z.H.Zhong, *Finite Element Procedures for Contact Impact Problems*, Oxford University Press, New York, 1993.

[28] A.A. Arulkar, P.P. Ritapure, *Computer Simulation to Study Effect of Process Parameters on Erosive Wear of Composite*, International Journal for Scientific Research & Development, vol. 5, iss. 8, pp. 206-209, 2017.

[29] H.M. Clark, *On the impact rate and impact energy of particles in a slurry pot erosion tester*, Wear, vol. 147, iss. 1, pp. 165–183, 1991, doi: 10.1016/0043-1648(91)90127-G

[30] R.S. Lynn, K.K. Wong, H.M. Clark, *On the Particle Size Effect in Slurry Erosion*, Wear, vol. 149, iss. 1-2, pp. 55–71, 1991, doi: 10.1016/0043-1648(91)90364-Z

[31] H.M. Clark, *The influence of the flow field in slurry erosion*, Wear, vol. 152, iss. 2, pp. 223-240, 1992, doi: 10.1016/0043-1648(92)90122-O

[32] H.M. Clark, *Specimen Diameter, Impact Velocity, Erosion Rate and Density in a Slurry Pot Erosion Tester*, Wear, vol. 162–164, pp. 669–678, 1993, doi: 10.1016/0043-1648(93)90065-T

[33] H.M. Clark, R.B. Hartwich, *A Re-Examination of the Particle Size Effect in Slurry Erosion*, Wear, vol. 248, iss. 1–2, pp. 147–161, 2001, doi: 10.1016/S0043-1648(00)00556-1

[34] A.Ramadhan Al-Obaidi, R. Mishra, *Experimental Investigation of the Effect of Air Injection on Performance and Detection of Cavitation in the Centrifugal Pump Based on Vibration Technique*, Arabian Journal for Science and Engineering, vol. 45, pp. 5657–5671, 2020, doi: 10.1007/s13369-020-04509-3

[35] A.R. Al-Obaidi, *Experimental comparative investigations to evaluate cavitation conditions within a centrifugal pump based on vibration and acoustic analyses techniques*, Archives Of Acoustics, vol. 45, no. 3, pp. 541–556, 2020, doi: 10.24425/aoa.2020.134070

[36] A.R. Al-Obaidi, *Influence of guide vanes on the flow fields and performance of axial pump under unsteady flow conditions: Numerical study*, Journal of mechanical engineering and sciences (JMES), vol. 14, iss. 2, pp. 6570 – 6593, 2020.

[37] G.R. Desale, B.K. Gandhi, S.C. Jain, *Particle Size Effects on The Slurry Erosion of Aluminium Alloy (AA 6063)*, Wear, vol. 266, iss. 11-12, pp. 1066-1071,2009, doi: 10.1016/j.wear.2009.01.002

[38] G.R. Desale, B.K. Gandhi, S.C. Jain, *Slurry erosion of ductile materials under normal impact condition*, Wear, vol. 264, iss. 3-4, pp. 322–330, 2008, doi: 10.1016/j.wear.2007.03.022

[39] V.V. Shanbhag, B.F. Rolfe, J.M. Griffin, N. Arunachalam , M.P. Pereira, Understanding galling wear initiation and progression using force and acoustic emissions sensors, Wear, vol. 436–437, 2019, doi: 10.1016/j.wear.2019.202991

[40] A.K. Rai, A. Kumar, T. Staubli, *Analytical modelling and mechanism of hydro-abrasive erosion in pelton buckets*, Wear, vol. 436–437, 2019, doi: 10.1016/j.wear.2019.203003

[41] B. Podgornik, F. Kafexhiu, A. Nevosad, E. Badisch, *Influence of surface roughness and phosphate coating on galling resistance of medium-grade carbon steel*, wear, vol. 446–447, 2020, doi: 10.1016/j.wear.2019.203180